Simulation of Fermionic Evaporative Cooling Using the Direct Simulation Monte Carlo Method

Haoyang Liu
Department of Physics, The Chinese University of Hong Kong

November 30, 2024

Abstract

The simulation of ultra cold fermionic system is challenging due to the significant quantum effects inherent in these systems. But the system is fundamentally described by the quantum Boltzmann equation, which solution provides a statistical description for modeling particle's behavior. In this paper, we introduce Direct Simulation Monte Carlo method as an efficient method for solving the Boltzmann equation in the context of cold atomic systems. Finally we successfully simulate fermionic evaporative cooling, confirming its applicability to ultra cold systems by using this method. This study not only demonstrates the feasibility of Direct Simulation Monte Carlo for ultra cold simulations but also highlights its potential as a fast and versatile tool for exploring quantum statistical phenomena.

I Introduction

With the successful realizations of Bose-Einstein condensation [1] and Fermi degeneracy [2], Atomic, Molecular, and Optical(AMO) physics has emerged as a rapidly advancing field with profound implications for quantum computing [3], precision measurement [4], and fundamental research in quantum mechanics [5]. These developments highlight the need for robust simulation techniques that can accurately model the behavior and interactions of ultra cold atomic systems, especially in complex cooling processes.

Among existing cooling methods in AMO, evaporative cooling is extensively utilized [6]. However, simulating fermionic systems at ultralow temperatures remains challenging due to the intricate inter-particle interactions which often defy conventional computational approaches. In 1970, G.A.Bird introduced the Direct Simulation Monte Carlo (DSMC) method [7], which has since proven effective in modeling dilute particle systems through a stochastic approach by solving the Boltzmann equation [8]. DSMC's capability to handle complex collision dynamics suggests it may offer a viable pathway for modeling ultra cold atoms within AMO physics, where traditional techniques fall short.

This study aims to apply DSMC to do the simulation of evaporative cooling of ultra cold fermions, then assess the method's feasibility and precision. By evaluating DSMC's performance in simulation, we contributes a new way into developing more sophisticated simulation methodologies for AMO physics.

The rest of this paper is organized as follows. Sec.II presents the theoretical model of quantum Boltzmann equation and two numerical methods: Molecular Dynamics and Direct Simulation Monte Carlo. Main results of those two methods are shown in Sec.III with some limitations and new questions for future study in Sec.IV. Final remarks and conclusions are drawn in Sec.V.

II Methods

II.A Quantum Boltzmann Equation

The dynamics of ultra cold fermions is governed by the quantum Boltzmann equation, which provides a statistical description of rarefied gases in phase space in-

cluding position and momentum [9]. From Boltzmann equation, the many body system could be described by a single-particle phase space distribution function $f(\mathbf{r}, \mathbf{p}, t)$, which is defined as:

$$\int d^3r\, d^3p\, f(\mathbf{r}, \mathbf{p}, t) = N, \tag{1}$$

with phase space position and momentum coordinates $(\mathbf{r}, \mathbf{p})$. Then the Boltzmann equation could be written as:

$$\left(\frac{\partial}{\partial t} + \frac{\mathbf{p}}{m} \cdot \nabla_r - \nabla_r V(\mathbf{r}) \cdot \nabla_p\right) f(\mathbf{r}, \mathbf{p}, t) = \mathcal{I}[f], \tag{2}$$

where m denotes the molecular mass, $V(\mathbf{r})$ denotes the trap potential and the number of molecules in system is denoted by N. The meaning of these four terms $\frac{\partial f}{\partial t}$, $\frac{p}{m} \cdot \nabla_r f$, $-\nabla_r V(r) \cdot \nabla_p f$, $\mathcal{I}[f]$ are the time evolution of the distribution function, the effect of particle transport in position space, the effect of external forces on the change of momentum and the impact of inter-particle collisions on the distribution function which is called the collision term or collision integral.

When temperature is lower than the Fermi temperature T_F during evaporative cooling, the Pauli blocking must be included into collision term, then the collision term could be written as: [10]

$$\begin{aligned}\mathcal{I}[f] = \int \frac{d^3p_1}{m} |\mathbf{p} - \mathbf{p}_1| \int d\Omega' \frac{d\sigma}{d\Omega'} \\ \times \left[f' f_1' (1 - h^3 f)(1 - h^3 f_1) \right. \\ \left. - f f_1 (1 - h^3 f')(1 - h^3 f_1')\right],\end{aligned} \tag{3}$$

where $d\sigma/d\Omega$ is the differential cross section and the shorthand notation $f_1 = f(\mathbf{r}, \mathbf{p}_1, t)$ and $f' = f(\mathbf{r}, \mathbf{p}', t)$ are used. When the phase space densities (PSD) have order $\rho_{PSD} \gtrsim 0.1$, the Pauli blocking factors $(1 - h^3 f)$ become significant in simulation, where ρ_{PSD} is defined as:

$$\rho_{PSD} = \langle n \rangle \lambda_{th}^3, \tag{4}$$

which compares the ensemble averaged number density $\langle n \rangle$ against the cubed thermal de Broglie wavelength $\lambda_{th} = h/\sqrt{2\pi m k_B T}$ with h denoting Planck's constant, k_B denoting Boltzmann's constant and T denoting the temperature of Fermi gases.

Direct numerical solution of this 6-dimensional phase space distribution is extremely expensive. So we adopt the approximation [7] where $f(\mathbf{r}, \mathbf{p})$ is discretized in phase space points as simulation particles:

$$f(\mathbf{r}, \mathbf{p}) \approx \xi \sum_{k=1}^{N_{\text{sim}}} \delta^3(\mathbf{r} - \mathbf{r}_k) \delta^3(\mathbf{p} - \mathbf{p}_k), \tag{5}$$

where $\xi = N/N_{sim}$ is the ratio of the actual number of particles N to simulation number of particles N_{sim}. Because the number of particles in AMO physics is not very large, so we set $\xi = 1$ in our simulation even though at traditional DSMC $\xi < 1$.

II.B Molecular Dynamics

To verify the feasibility and effectiveness of DSMC, we use Molecular Dynamics (MD) simulation as a benchmark in this project. MD is a *ab initio* method, where at each time interval, the forces acting on individual molecules are computed. These forces, applied through Newton's laws of motion, yield the resulting accelerations, allowing for systematic updates to molecular velocities and displacements.

The gas is confined in a crossed optical dipole trap (xODT) with 2 perpendicular intersecting Gaussian beams, modelled by the potential $V_{ODT}(\mathbf{r})$ defined as [6]:

$$\begin{aligned}V_{\text{ODT}}(\mathbf{r}) = -\frac{2\alpha_1 P_1 \exp\left(-\frac{2y^2}{w_{1,y}(x)} - \frac{2z^2}{w_{1,z}(x)}\right)}{\pi w_{1,y}(x) w_{1,z}(x)} \\ - \frac{2\alpha_2 P_2 \exp\left(-\frac{2x^2}{w_{2,x}(y)} - \frac{2z^2}{w_{2,z}(y)}\right)}{\pi w_{2,x}(y) w_{2,z}(y)},\end{aligned} \tag{6}$$

Each beam's laser power is denoted by P_i and the molecular polarizability is denoted by α_i. $\omega_{\mu,i}(r)$ is represented as:

$$\omega_{\mu,i}(r) = W_{\mu,i} \sqrt{1 + \frac{r^2}{R_{\mu,i}^2}}, \tag{7}$$

where $R_{\mu,i} = \pi W_{\mu,i}^2/\lambda$ denoting the Rayleigh length and $W_{\mu,i}$ is the beam width of wavelength λ.

The forces generated by the xODT are calculated at Appendix B.

In other way, this Gaussion trap V_{ODT} could be seen as harmonic around the trap minima:

$$V_{\text{harm}}(r) = \frac{1}{2} m \sum_{\nu} \omega_\nu^2 r_\nu^2, \tag{8}$$

where ω_ν are the harmonic trap frequencies along coordinate axis ν and they are calculated at Appendix A.

For intermolecular forces, we employ the Lennard-Jones (LJ) potential to model the interactions between two molecules. LJ potential is defined as:

$$V_{\mathrm{LJ}}(r) = 4\epsilon\left[\left(\frac{\sigma}{r}\right)^{12} - \left(\frac{\sigma}{r}\right)^{6}\right], \tag{9}$$

where r is the distance between two particles, ϵ is the depth of the potential indicating the strength of the interaction between particles and σ is a scale parameter which characterizes the effective size of the particles.

LJ potential captures both the attractive and repulsive forces based on the distance between two particles, making it well suited for simulating van der Waals interactions.

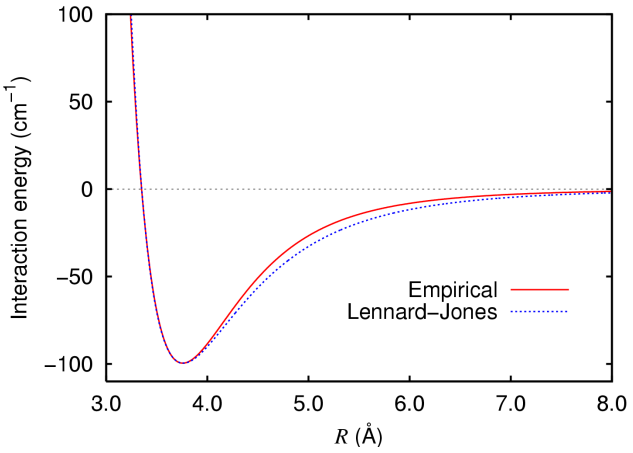

FIG. 1. The interaction energy as a function of interatomic distance R. The red solid line represents an empirical potential, while the blue dotted line represents the Lennard-Jones potential V_{LJ}. From this figure we could see that the LJ potential fits almost perfectly to the actual physical situation.

During evaporative cooling, the trap depth which promotes the loss of energetic molecules should be lowered by reducing the trap power. During this process, the trap powers follow Eq.10 to achieve a rapid drop followed by a gradual levelling off:

$$P_i(t) = P_i(0) - \Delta P_i\left(\frac{1-e^{-t/\tau}}{1-e^{-t_d/\tau}}\right), \tag{10}$$

where ΔP_i is the change in laser power of beam i, t_d denotes the characteristic decay time and τ denotes the forced evaporation time.

To update the velocities and displacements of particles, we apply the Velocity Verlet symplectic algorithm [11]. This algorithm is advantageous due to its stability and ability to conserve energy over long simulation periods, making it ideal for Molecular Dynamics simulation. At each time step, the Velocity Verlet algorithm calculates new particle positions and velocities by integrating Newton's equations of motion, ensuring accurate and consistent updates based on the xODT and Lennard-Jones potential. The update strategy of the Velocity Verlet algorithm is shown in Eq.11.

$$v_k(t+\frac{\Delta t}{2}) = v_k(t) + F_k(r_k)\frac{\Delta t}{2m}, \tag{11a}$$

$$r'_k = r_k(t) + v_k(t+\frac{\Delta t}{2})\Delta t, \tag{11b}$$

$$r_k(t+\Delta t) = r'_k, \tag{11c}$$

$$v_k(t+\Delta t) = v_k(t+\frac{\Delta t}{2}) + F_k(r'_k)\frac{\Delta t}{2m}. \tag{11d}$$

A position space cutoff scheme is used to effectively simulate the evaporative cooling following a lowering of the trap depth. A particle is taken as evaporated from this xODT trap if it goes past a position which is 6 times the thermal width of the initial cloud $\sqrt{k_B T_0/m\omega_\nu^2(0)}$ from the trap minimum:

$$|r_\nu - r_{\nu,\min}| > 6\sqrt{\frac{k_B T_0}{m\omega_\nu^2(0)}}, \tag{12}$$

where T_0 denotes the initial equilibrium temperature setting at beginning during simulation, $r_{\nu,\min}$ denotes the position of the trap minimum along axis ν and it was set to be 0 in our simulation.

II.C Direct Simulation Monte Carlo

This section we will introduce Direct Simulation Monte Carlo method. DSMC is an efficient alternative for simulating a dilute particle system. It can be viewed as simplified Molecular Dynamics or Monte Carlo method when solving Boltzmann equation. Rather than calculating collisions exactly as in Molecular Dynamics, DSMC generates collisions stochastically with scattering rates and post collision momentum distributions determined from the kinetic theory of a dilute gas. Although DSMC simulations are not correct at a length scale of an atomic diameter, they are proved to be accurate at scales smaller than that of a mean free path [7].

The workflow of DSMC method proceeds as follows. Initially, particle velocities are generated based on the Maxwell-Boltzmann distribution, while particle positions are initialized in a fixed-point grid arrangement. Then during each time step δt, the forces acting on the particles are computed within the xODT trap, a process referred to as free-stream kinetics. For this step, the Velocity Verlet symplectic algorithm 11 can be employed to update particle velocities and displacements, analogous to approaches used in Molecular Dynamics simulations.

To account for inter particle interactions or the collision term in quantum Boltzmann equation, the spatial grid is built every δt in two steps. First step is the construction of a master grid, consisting of uniform volume cells whcih span the simulation volume surrounding the test particle ensemble. At second step, the resolution of the spatial grid is then refined with an octree algorithm [12] which recursively subdivides each master grid cell into eight octants, terminating only when each cell has at most N_{cell}^{max} test particles. In this project we use $N_{cell}^{max} = 30$. The octree refinement of an initial master grid is illustrated in Fig. 2.

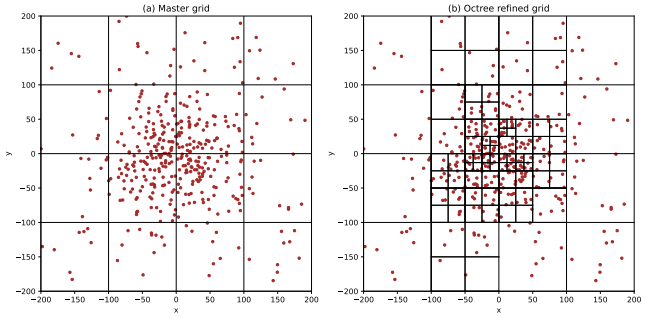

FIG. 2. 2-d visualisation of the octree algorithm refinement (b) applied to the master grid (a). There are initially 16 master grid cells with $N = 400$ and $N_{max}^{cell} = 3$, with Gaussian distributed points in arbitrary units in this figure. We could see that in (b) the number of particles in each grid is roughly the same due to the adaptive division of the master grid.

In DSMC, the collisions occur only within the grid cells, with the result that they depart from the phase-space volume element d^3rd^3p at the rate $\mathcal{I}^{\text{out}}[f]$, where

$$\mathcal{I}^{\text{out}}[f] = -\int \frac{d^3p_1}{m} |\mathbf{p} - \mathbf{p}_1| \int d\Omega' \frac{d\sigma}{d\Omega'} \tag{13}$$

$$\times f f_1 (1 - h^3 f')(1 - h^3 f'_1). \tag{14}$$

In collision occurrences step, a collision proceeds between test particles i and j, with probability [13]:

$$P_{ij} \approx \xi \frac{\delta t}{m \Delta V_{\text{cell}}} |\mathbf{p}_{ij}| \sigma(\mathbf{p}_{ij}), \tag{15}$$

where $\mathbf{p}_{ij} = \mathbf{p}_i - \mathbf{p}j$ and here we set collision cross section $\sigma(\mathbf{p}_{ij}) = \pi\sigma^2$ where σ is the scale parameter in Lennard-Jones potential.

To simulate two body loss which against the system into Fermi degeneracy, the cross section could be written as:

$$\sigma(ij) = \sigma_{eff} + \sigma_{loss}, \tag{16}$$

where σ_{eff} denotes elastic cross section and σ_{loss} denotes inelastic cross section. When we use σ_{loss} in collision section, two particles are moved from the xODT trap, as we have observed in experiments about the phenomenon of two body loss.

Quantum statistics or Pauli blocking factor require an additional accept reject step [14], where the sampled post collision momenta are only accepted with probability

$$P'_{ij} = (1 - h^3 f'_i)(1 - h^3 f'_j), \tag{17}$$

otherwise, no collision is said to have occurred.

Sampling f' in Eq.17 is problematic because the particle distributions f'_i and f'_j are discretised in the simulation. So we change the δ-function to Gaussian convolution kernel [14]. These kernels are taken to have spatial width ϑ_ν along axis ν and momentum width ϑ_p. So the discretization noise could be smoothed out while the distribution function remains physically consistent. These criteria are determined by the conditions: [15]

$$\vartheta_p \bar{\vartheta}_q \gg h\xi^{1/3}, \tag{18a}$$

$$\vartheta_\nu \ll R_\nu \frac{T}{T_F}, \tag{18b}$$

$$\vartheta_p \ll p_F \frac{T}{T_F}. \tag{18c}$$

where $E_F = k_B T_F = \hbar\bar{\omega}(6N)^{1/3}$ [16] denotes Fermi temperature, $p_F = \sqrt{2mE_F}$ denotes the Fermi momentum and $R\nu = \sqrt{2E_F/(m\omega_\nu^2)}$ are the Thomas-Fermi redii [17]. $\bar{\omega}$ and $\bar{\varsigma}_q$ denote geometric means. We use widths defined by the geomatic means of those upper and lower

bounds like:

$$\vartheta_\nu = \sqrt{\left(\frac{\hbar}{m\omega_\nu}\right)^{1/2}\left(R_\nu \frac{T}{T_F}\right)}, \tag{19a}$$

$$\vartheta_p = \sqrt{(m\hbar\overline{\omega})^{1/2}\left(p_F \frac{T}{T_F}\right)}. \tag{19b}$$

Then the convolution kernels are defined as:

$$\delta^3(\mathbf{r}-\mathbf{r}_k) \to c_r(\mathbf{r}-\mathbf{r}_k) \equiv \prod_{\nu=1}^{3} \frac{e^{-(r-r_k)^2/\vartheta_\nu^2}}{\sqrt{\pi\vartheta_\nu^2}}, \tag{20a}$$

$$\delta^3(\mathbf{p}-\mathbf{p}_k) \to c_p(\mathbf{p}-\mathbf{p}_k) \equiv \prod_{\nu=1}^{3} \frac{e^{-(p-p_k)^2/\vartheta_{p_\nu}^2}}{\sqrt{\pi\vartheta_{p_\nu}^2}}. \tag{20b}$$

which when used in Eq.5, constitute a continuous distribution Eq.17.

In evaporative cooling theory [6], $\log_{10}\rho_{\mathrm{PSD}}/\log_{10} N$ describes the forced evaporation trajectory where ρ_{PSD} is the phase space density and N is the particle number of this system. So we could extract an evaporation efficiency through a linear fit of its decrease [18]:

$$\mathcal{E}_{\mathrm{evap}} = -\frac{\partial \log_{10}\rho_{\mathrm{PSD}}}{\partial \log_{10} N}. \tag{21}$$

We could check the correctness of those two methods by comparing Eq.21 with the simulation data.

III Results

The laser parameter values for potential in this study are listed in Tab. I with the initial trap potential energy surface shown in Fig. 3.

The plot of trap potential energy surface is a slice along $y = 0$ and shows the initial trap depth is about $2.5\mu K$.

The main results of this simulation are presented demonstrate the accuracy and reliability of DSMC and by changing some parameters in this method, we also get another interesting findings.

TABLE I. Table of parameter values for the potential confining a gas of fermionic $^{23}Na^{40}K$ molecules. h denotes Planck's constant.

Parameter	Symbol	Value	Unit
Beam 1 vertical width	$W_{1,z}$	57.5	µm
Beam 1 horizontal width	$W_{1,\perp}$	113	µm
Beam 1 wavelength	λ_1	1064	nm
Beam 1 power	P_1	0.242	W
Polarizability in beam 1	α_1	$2.79\times10^{-3}h$	$\mathrm{m^2\,J\,W^{-1}}$
Beam 2 vertical width	$W_{2,z}$	45	µm
Beam 2 horizontal width	$W_{2,\perp}$	156	µm
Beam 2 wavelength	λ_2	1064	nm
Beam 2 power	P_2	0.253	W
Polarizability in beam 2	α_2	$2.79\times10^{-3}h$	$\mathrm{m^2\,J\,W^{-1}}$

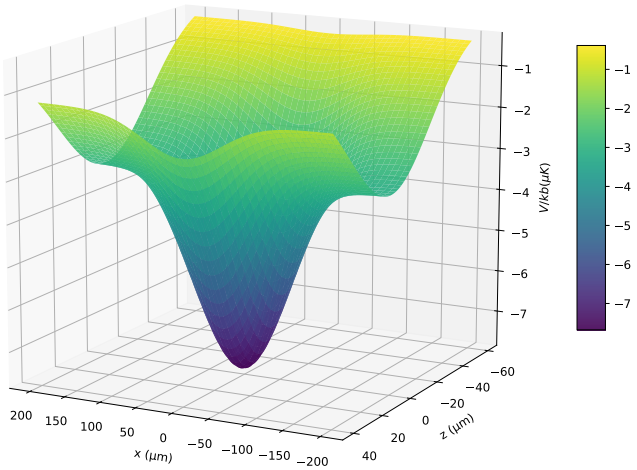

FIG. 3. The xODT potential energy surface $V(\mathbf{r})$, plotted as a function of coordinates x and z along $y = 0$, utilizing the trap parameters of Tab. I.

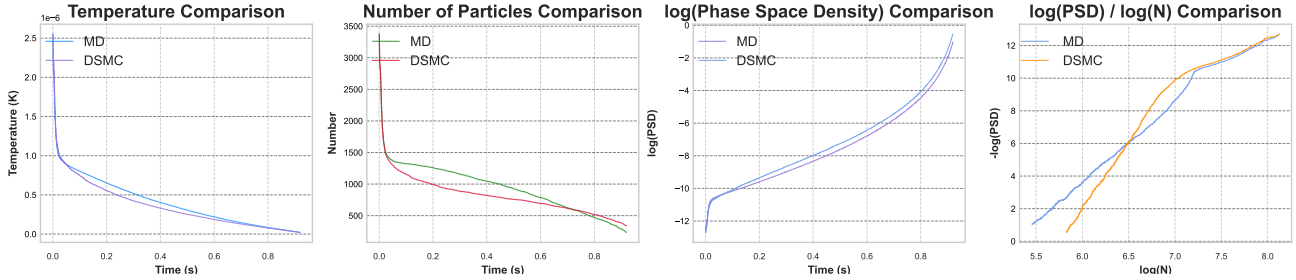

FIG. 4. The comparison of results between Molecular Dynamics and Direct Simulation Monte Carlo. The first plot is about temperature, the second is about number of particles in trap, the third is about phase space density and the final one is about log ρPSD versus log molecule number.

From Fig. 4, we could see the temperature, phase space density of two methods, Molecular Dynamics and Direct Simulation Monte Carlo, are extremely similar. But the number of particles in trap have a little different. The possible reason for this may be that DSMC uses stochastic collisions while MD uses *ab initio* for calculations, so there are some differences in the intermediate processes. The final plot has a linear fit excluding the end part, which means the evaporation efficiency is a constant in the process. That proves our simulation is correct, and the reason of why the end part is not good maybe at the end of simulation, the particle number become smaller and stochasticity of simulation increases.

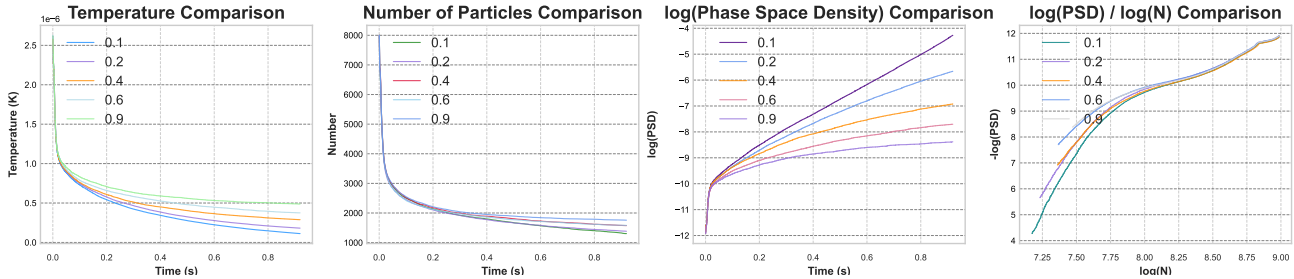

FIG. 5. The comparison of different Direct Simulation Monte Carlo results by changing $\Delta P_i/P_i$ to 0.9, 0.8, 0.6, 0.4, 0.1. Legend **0.1** denotes $\Delta P_i/P_i = 0.9$ which means the final trap depth versus initial trap depth is 0.1 and another legend are same. The first plot is about temperature, the second is about number of particles in trap, the third is about log of phase space density and the final one is about log ρ_{PSD} versus log molecule number.

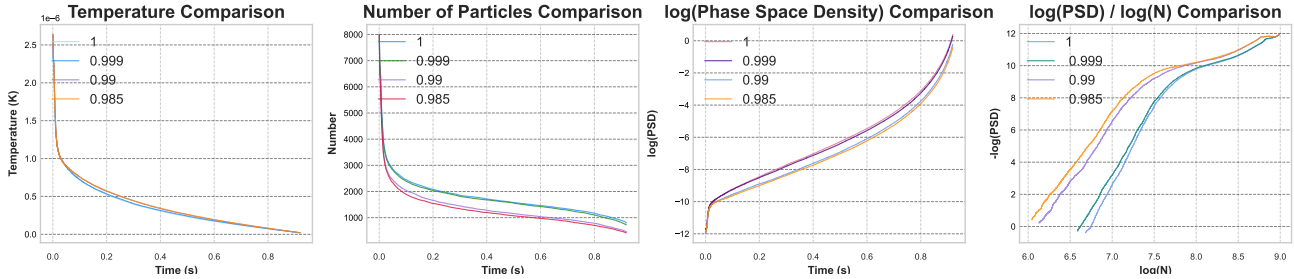

FIG. 6. The comparison of different Direct Simulation Monte Carlo results by changing the ratio of σ_{eff} and σ_{ij}. Legend **0.985** means $\sigma_{eff}/\sigma_{ij} = 0.985$ and another legend are same. The first plot is about temperature, the second is about number of particles in trap, the third is about log of phase space density and the final one is about log ρ_{PSD} versus log molecule number.

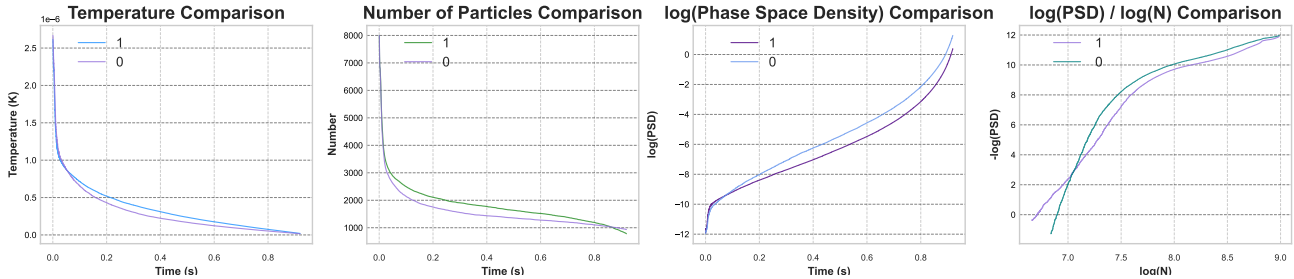

FIG. 7. The comparison of different Direct Simulation Monte Carlo results about adding or not adding Pauli blocking factor in simulation. Legend **0** denotes not add and **1** denotes add. The first plot is about temperature, the second is about number of particles in trap, the third is about log of phase space density and the final one is about log ρ_{PSD} versus log molecule number.

Fig. 5 shows different results when we use different $1 - \Delta P_i/Pi$, which could be seen as the depth of trap. From this figure, we could find lower trap depth could get higher ρ_{PSD}, or become Fermi degeneracy faster, which conforms to physical intuition.

Fig. 6 shows different results when we change the ratio of elastic cross section σ_{eff} and total cross section σ_{ij}. From this figure, we could see larger ratio, which means two body loss effect become smaller in simulation, could get higher ρ_{PSD} and this phenomenon conforms to theoretical derivation and experimental phenomena. In fact, in ultra cold atom experiments, we have to lower the two body loss frequency as much as possible to achieve better Fermi degeneracy or Bose-Einstein condensation and a common way is Microwave Shielding[19].

Fig. 7 shows different results about adding Pauli blocking factor or doing nothing in simulation. From this figure, we could see when adding the effect of Pauli blocking, the number of particles in trap is become larger and ρ_{PSD} become lower. Because Pauli blocking will against the interaction between particles, so it's hard to get into Fermi degeneracy for this system. This result also fits theoretical derivation and experimental phenomena.

IV Discussion

We use Direct Simulation Monte Carlo to simulate the evaporative cooling of ultra cold fermions. From the simulation results, this method could be seen effective for modelling such systems. However, several challenges were encountered during the study.

Firstly, in this study, we set $N_{\text{sim}} = N$, resulting in a weighting factor $\xi = 1$ when discretizing the quantum Boltzmann equation into phase-space points. But in traditional DSMC, one simulation particle or phase-space point often represents multiple physical particles or $\xi < 1$. While reducing ξ like using fewer simulation particles to represent more physical particles could be a practical way to simulate larger systems, it raises concerns about whether the simulation particles would still accurately capture the physical molecular dynamics, particularly in terms of particle loss. This potential discrepancy highlights the need for further validation when employing weighting factors smaller than one.

Additionally, our study focuses on the simulation of Fermi degeneracy. Due to the presence of the Pauli blocking factor, we can incorporate an extra accept-reject step when handling the collision term in DSMC. This modification accounts for the quantum statistical effects specific to fermions. However, for bosons and corresponding Bose-Einstein condensation, the situation could be more complex and presents greater challenges due to the unique properties of the boson. Therefore, how to use DSMC do simulation of ultra cold bosons is a significant issue that future research should address.

Finally, in order to simulate the evaporative cooling experiment in a more physical way, we need to consider the effects of gravity and background radiation. What's more, we can add more quantum efficiency to the DSMC collision terms for a better simulation results.

In conclusion, DSMC matches the results of MD and achieves more good results in evaporative cooling simulation of fermions, which proves that DSMC can be used as a new simulation method in AMO physics. Of course, our study is not sufficient and there is still much challenge to conquer in future, such as incorporating environmental effects to better fit the experiment and exploring the simulation of bosons.

V Conclusion

In this study, we successfully demonstrate the feasibility of using Direct Simulation Monte Carlo method to simulate evaporative cooling experiments of fermionic. This work provides a new approach to modeling ultra cold atomic systems.

However, we also encountered some problems in the simulation, including some mistakes about gravity, and eventually had to remove the effect of it. So we obtain a better result by simulating a more idealised model without gravity and background radiation.

Despite these challenges, the results obtained in this study demonstrate the promise of DSMC as a tool for ultra cold atom simulations, particularly for exploring complex quantum phenomena in ultra cold systems and AMO physics.

Appendix A The harmonic trap approximation

The harmonic trap potential V_{ODT} could be expanded up to second order around the trap minima as:

$$V_{\text{harm}}(r) = \frac{1}{2} m \sum_{\nu} \omega_{\nu}^2 r_{\nu}^2, \tag{22}$$

where the coefficients are calculated as:

$$A_x = \frac{\alpha_1 P_1 \lambda_1^2 \left(W_{1,y}^4 + W_{1,z}^4\right)}{\pi^3 W_{1,y}^5 W_{1,z}^5} + \frac{4\alpha_2 P_2}{\pi W_{2,x}^3 W_{2,z}}, \tag{23a}$$

$$A_y = \frac{4\alpha_1 P_1}{\pi W_{1,y}^3 W_{1,z}} + \frac{\alpha_2 P_2 \lambda_2^2 \left(W_{2,x}^4 + W_{2,z}^4\right)}{\pi^3 W_{2,x}^5 W_{2,z}^5}, \tag{23b}$$

$$A_z = \frac{4\alpha_1 P_1}{\pi W_{1,y}^3 W_{1,z}} + \frac{4\alpha_2 P_2}{\pi W_{2,x}^3 W_{2,z}}. \tag{23c}$$

then the harmonic trap frequencies are defined as:

$$\omega_{\nu}^2 = \frac{2A_{\nu}}{m}. \tag{24}$$

Appendix B Trapping Force

The effective force of the trapping potential for every molecule is given as $\mathbf{F} = -\nabla V(\mathbf{r})$, which we compute in this section explicitly. For convenience, we decompose $V_{ODT}(\mathbf{r})$ by defining each cross propagating beam individually:

$$V_{\text{ODT},1}(\mathbf{r}) = -\frac{2\alpha_1 P_1 \exp\left(-\frac{2y^2}{w_{1,y}(x)} - \frac{2z^2}{w_{1,z}(x)}\right)}{\pi w_{1,y}(x) w_{1,z}(x)}, \tag{25a}$$

$$V_{\text{ODT},2}(\mathbf{r}) = -\frac{2\alpha_2 P_2 \exp\left(-\frac{2x^2}{w_{2,x}(y)} - \frac{2z^2}{w_{2,z}(y)}\right)}{\pi w_{2,x}(y) w_{2,z}(y)}. \tag{25b}$$

Then taking the gradients of each term, we obtain:

$$\frac{-\nabla V_{\text{ODT},1}(\mathbf{r})}{V_{\text{ODT},1}(\mathbf{r})} = \begin{pmatrix} \frac{2}{x} + \frac{4\pi^4}{x}\left(\frac{W_{1,y}^6 y^2}{(\pi^2 W_{1,y}^4 + \lambda_1^2 x^2)^2} + \frac{W_{1,z}^6 z^2}{(\pi^2 W_{1,z}^4 + \lambda_1^2 x^2)^2}\right) - \frac{\pi^2}{x}\left(\frac{W_{1,y}^4 + 4W_{1,y}^2 y^2}{\pi^2 W_{1,y}^4 + \lambda_1^2 x^2} + \frac{W_{1,z}^4 + 4W_{1,z}^2 z^2}{\pi^2 W_{1,z}^4 + \lambda_1^2 x^2}\right) \\ \frac{4\pi^2 W_{1,y}^2 y}{\pi^2 W_{1,y}^4 + \lambda_1^2 x^2} \\ \frac{4\pi^2 W_{1,z}^2 z}{\pi^2 W_{1,z}^4 + \lambda_1^2 x^2} \end{pmatrix}, \tag{26a}$$

$$\frac{-\nabla V_{\text{ODT},2}(\mathbf{r})}{V_{\text{ODT},2}(\mathbf{r})} = \begin{pmatrix} \frac{4\pi^2 W_{2,x}^2 x}{\pi^2 W_{2,x}^4 + \lambda_2^2 y^2} \\ \frac{2}{y} + \frac{4\pi^4}{y}\left(\frac{W_{2,x}^6 x^2}{(\pi^2 W_{2,x}^4 + \lambda_2^2 y^2)^2} + \frac{W_{2,z}^6 z^2}{(\pi^2 W_{2,z}^4 + \lambda_2^2 y^2)^2}\right) - \frac{\pi^2}{y}\left(\frac{W_{2,x}^4 + 4W_{2,x}^2 x^2}{\pi^2 W_{2,x}^4 + \lambda_2^2 y^2} + \frac{W_{2,z}^4 + 4W_{2,z}^2 z^2}{\pi^2 W_{2,z}^4 + \lambda_2^2 y^2}\right) \\ \frac{4\pi^2 W_{2,z}^2 z}{\pi^2 W_{2,z}^4 + \lambda_2^2 y^2} \end{pmatrix}, \tag{26b}$$

Although the expression above is algebraically nondivergent, the linear coordinates in the denominators of the first three gradient gradients may lead to numerical instability. Therefore, we also propose a first-order Taylor extension for the unstable coordinates in the components of the associated vectors:

$$\left[\nabla V_{\text{ODT},1}(\mathbf{r})\right]_x \approx \frac{2\alpha_1 P_1}{\pi W_{1,y} W_{1,z}}\left(\frac{1}{W_{1,y}^4} - \frac{4y^2}{W_{1,y}^6} + \frac{W_{1,z}^2 - 4z^2}{W_{1,z}^6}\right)\frac{\lambda_1^2}{\pi^2}\exp\left(-\frac{2y^2}{W_{1,y}^2} - \frac{2z^2}{W_{1,z}^2}\right)x + \mathcal{O}(x^2), \tag{27a}$$

$$\left[\nabla V_{\text{ODT},2}(\mathbf{r})\right]_y \approx \frac{2\alpha_2 P_2}{\pi W_{2,x} W_{2,z}}\left(\frac{1}{W_{2,x}^4} - \frac{4x^2}{W_{2,x}^6} + \frac{W_{2,z}^2 - 4z^2}{W_{2,z}^6}\right)\frac{\lambda_2^2}{\pi^2}\exp\left(-\frac{2x^2}{W_{2,x}^2} - \frac{2z^2}{W_{2,z}^2}\right)y + \mathcal{O}(y^2). \tag{27b}$$

We utilize these linearized gradients instead of those in Eq.26, for close-to-zero values of the respective coordinates in Monte Carlo simulations.

References

[1] K. Davis et al., *Bose-Einstein Condensation in a Gas of Sodium Atoms*, in: Phys. Rev. Lett. **75** (1995).

[2] B. DeMarco and D. S. Jin, *Onset of Fermi Degeneracy in a Trapped Atomic Gas*, in: Sci. **285**.5434 (1999).

[3] D. Jaksch and P. Zoller, *The Cold Atom Hubbard Toolbox*, in: Annals of Phys. **315**.1 (2005).

[4] Mark Kasevich and Steven Chu, *Atomic Interferometry Using Stimulated Raman Transitions*, in: Phys. Rev. Lett. **67**.2 (1991).

[5] Cheng Chin et al., *Feshbach Resonances in Ultracold Gases*, in: Rev. of Mod. Phys. **82**.2 (2010).

[6] Rudolf Grimm, Matthias Weidemüller, and Yurii B. Ovchinnikov, *Optical Dipole Traps for Neutral Atoms*, in: **42** (2000).

[7] G. A. Bird, *Direct Simulation and the Boltzmann Equation*, in: Phys. of Fluids **13** (1970).

[8] Hiroyuki Okamoto and Michio Nishida, *Numerical Analysis of the Rarefied Plume from an Arcjet Thruster: Effect of the Nozzle Exit Shape*, in: TRANSACTIONS OF THE JAPAN SOCIETY FOR AERONAUTICAL AND SPACE SCIENCES **44**.143 (2001).

[9] A. Bonasera, F. Gulminelli, and J. Molitoris, *The Boltzmann Equation at the Borderline. A Decade of Monte Carlo Simulations of a Quantum Kinetic Equation*, in: Phys. Reports **243**.1-2 (1994).

[10] L. W. Nordhiem and Ralph Howard Fowler, *On the Kinetic Method in the New Statistics and Application in the Electron Theory of Conductivity*, in: Proceedings of the Royal Society of London. Series A, Containing Papers of a Mathematical and Physical Character **119**.783 (1997).

[11] Loup Verlet, *Computer "Experiments" on Classical Fluids. I. Thermodynamical Properties of Lennard-Jones Molecules*, in: Phys. Rev. **159**.1 (1967).

[12] Wm. Randolph Franklin and Varol Akman, *Octree Data Structures and Creation by Stacking*, in: Computer-Generated Images (1985).

[13] Andrew Sykes and John Bohn, *Nonequilibrium Dynamics of an Ultracold Dipolar Gas*, in: Phys. Rev. A **91**.1 (2015).

[14] O. Goulko, F. Chevy, and C. Lobo, *Boltzmann Equation Simulation for a Trapped Fermi Gas of Atoms*, in: New Jou. of Phys. **14**.7 (2012).

[15] Thomas Lepers et al., *Numerical Solution of the Boltzmann Equation for the Collective Modes of Trapped Fermi Gases*, in: Phys. Rev. A **82** (2010).

[16] D. A. Butts and D. S. Rokhsar, *Trapped Fermi Gases*, in: Phys. Rev. A **55**.6 (1997).

[17] Stefano Giorgini, Lev P. Pitaevskii, and Sandro Stringari, *Theory of Ultracold Atomic Fermi Gases*, in: Rev. of Mod. Phys. **80**.4 (2008).

[18] Reuben R. W. Wang et al., *Simulations of Evaporation to Deep Fermi Degeneracy in Microwave-Shielded Molecules*, in: arXiv:2407.14466 (2024).

[19] Loïc Anderegg et al., *Observation of Microwave Shielding of Ultracold Molecules*, in: Sci. **373**.6556 (2021).